

Article

Simplified V/f Control Algorithm for Reduction of Current Fluctuations in Variable-Speed Operation of Induction Motors

Dong-Hyeok Son ¹ and Sung-An Kim ^{2,*} ¹ Sansystech, Busan 46918, Republic of Korea; dhs@sansystech.co.kr² Electric Power Machinery Team, Electric Propulsion Safety Technology Center, Ulsan Headquarters, Korea Marine Equipment Research Institute, Ulsan 44776, Republic of Korea

* Correspondence: sakim@komeri.re.kr

Abstract: This paper introduces a straightforward control strategy aimed at the reduction of current fluctuations within the low-frequency domain of open-loop V/f control in induction motor drives. Traditional control techniques necessitate the addition of a current compensator based on motor parameters and the use of digital filters such as band-pass or high-pass filters. These methods, however, rely on precise motor parameters and involve complex filter design and implementation. The proposed control is capable of suppressing current fluctuations without controlling the slip of the induction motor. The proposed control strategy generates the forced rotation angle and command input voltage using the V/f block and outputs the d-axis voltage using a proportional integral controller to keep the d-axis current constant at zero. The difference between the command input voltage and the d-axis voltage is applied as the q-axis voltage and then applied through SVPWM. In order to verify the effectiveness of the proposed control, the proposed control is implemented and analyzed using power simulation based on the results of the analysis of the causes of current fluctuations in the induction motor. Finally, the effect of suppressing current fluctuations of the induction motor is verified through experimental results. In the 10~19 Hz range, where the conventional V/f control method resulted in current fluctuation rates exceeding 10% and peaking at 113.3% at 13 Hz, the proposed method suppressed the fluctuation rate to below 8.6% across all frequencies. This paper validates the effectiveness of the proposed control strategy through these results.



Citation: Son, D.-H.; Kim, S.-A. Simplified V/f Control Algorithm for Reduction of Current Fluctuations in Variable-Speed Operation of Induction Motors. *Energies* **2024**, *17*, 1699. <https://doi.org/10.3390/en17071699>

Academic Editor: Ahmed Abu-Siada

Received: 25 February 2024

Revised: 27 March 2024

Accepted: 29 March 2024

Published: 2 April 2024



Copyright: © 2024 by the authors. Licensee MDPI, Basel, Switzerland. This article is an open access article distributed under the terms and conditions of the Creative Commons Attribution (CC BY) license (<https://creativecommons.org/licenses/by/4.0/>).

Keywords: current fluctuation; induction motor; PI controller; PWM inverter; V/f control

1. Introduction

In response to the escalating concerns about climate change and its potentially devastating effects, regulations are being fortified on a global scale. This international cooperative effort aims to not only mitigate the impacts of climate change but also stabilize the global climate system. As a direct consequence of these strengthened regulations, there has been a surge in research activities focusing on electrification systems in the industrial sector [1–3]. This research is pivotal in transitioning towards more sustainable and energy-efficient industrial practices. Among the various components of these electrification systems, induction motors stand out as a representative example among AC motors.

The characteristics of induction motors make them particularly useful in many industrial fields [4–9]. One of the key features of induction motors is their ability to operate at a constant speed without the need for a separate drive for operation. This simplifies the motor design and reduces the complexity of the motor control systems. However, while the ability to operate at a constant speed can be advantageous in certain applications, it also presents a challenge. Specifically, when induction motors operate at a constant speed under varying loads, it can result in significant energy loss. This is because the motor may be operating at a higher speed than necessary for the given load, leading to unnecessary energy consumption. To address this issue, drives are applied to induction motors to enable variable-speed operation [10–14]. By

allowing the motor speed to vary according to the load, these drives can significantly improve the energy efficiency of the system. Therefore, the research and development of these drives and their integration into induction motors is an active area of research, driven by the global push towards energy efficiency and sustainability.

In situations where a high degree of dynamic performance is necessitated, closed-loop control methodologies such as field-oriented control (FOC) or direct-torque control (DTC) are predominantly employed [15–19]. These control methodologies are highly effective in optimizing the performance metrics of induction motors, ensuring stability under a wide array of load conditions. They achieve this by continuously monitoring the system's output and adjusting the input accordingly, thereby maintaining a desired system behavior. However, the implementation of such sophisticated control strategies requires a drive system that encompasses high-performance micro-controller units (MCU), a variety of sensors, and passive components. These elements, while integral to the functionality of the control system, contribute to an increase in the overall cost of the system. This cost factor can be a significant deterrent in certain applications, particularly those that are cost-sensitive.

To circumvent issues such as cost escalations, open-loop control is often preferred over closed-loop control in certain applications. In an open-loop system, the control action is independent of the output. This means that the system does not adjust itself based on the output, which simplifies the control mechanism. A representative example of an open-loop control method is V/f control. This method is particularly advantageous as it significantly reduces implementation costs because it does not necessitate the use of sensors and high-performance MCUs [20–24]. This makes V/f control a cost-effective solution for controlling induction motors.

V/f control finds its application in systems such as pumps and fans, where the load torque is proportional to the square of the operating frequency [25]. This relationship between load torque and operating frequency makes V/f control an ideal choice for these applications. However, in light-load and low-speed environments, V/f control can lead to continuous vibrations. These vibrations can cause seriously distorted output currents, leading to thermal damage due to overcurrent in the motor and potential damage to the power semiconductors in the drive [26]. This is a significant concern as it can lead to system failure and costly repairs.

The vibration stability of V/f control was evaluated by providing global convergence stability conditions. These conditions are in relation to motor parameters, operating slip, and synchronous frequency. The evaluation was based on small-signal linearization and pole-position evaluation using the frequency–voltage plane or the torque–frequency plane [27–30]. This evaluation provides valuable insights into the stability of the system under various operating conditions and can guide the design of more stable and reliable control systems.

The conventional solution to suppress vibration, a common issue in the operation of induction motors, is to apply active damping technology. This technology is fundamentally based on current feedback, a method that uses the motor's current to adjust its operation and reduce vibrations. This approach has been widely adopted due to its effectiveness and simplicity.

In reference [29], a specific implementation of this solution is discussed. Here, two proportional integral (PI) controls are used. These controls take the current magnitude and angle as input. Based on these inputs, the controls adjust the amplitude and frequency of the stator voltage. This adjustment allows the motor to operate more smoothly, reducing vibrations and improving overall performance. A similar PI approach is implemented in [30]. In this case, the differential current, which is the difference between the actual and desired current, influences the amplitude of the stator voltage. By adjusting the stator voltage based on the differential current, the system can effectively control the motor's operation, leading to improved performance and reduced vibrations.

In [8], the direct-axis current is filtered with a band-pass filter (BPF). This filter allows only a specific range of frequencies to pass through, effectively filtering out unwanted noise

and fluctuations. At low speeds, the output of the BPF alters the amplitude of the stator voltage, while at high speeds, it changes the frequency. This dynamic adjustment of the stator voltage helps to maintain stable motor operation across a wide range of speeds.

In [31], both the direct-axis current and quadrature-axis current are sent to a BPF. The filtered values are then used to adjust the frequency of the stator voltage. This method allows for precise control of the stator voltage frequency, leading to improved motor performance. In [32], the same scheme as [31] is used, but a high-pass filter (HPF) is used instead of a BPF. The HPF allows only frequencies higher than a certain cutoff frequency to pass through. This can be particularly useful in applications where it is necessary to eliminate low-frequency noise and fluctuations.

In [33], various strategies are tested. The HPF is applied to the quadrature-axis current and used to modify the direct-axis voltage, an HPF is applied to the direct-axis current and used to modify the quadrature-axis voltage, and finally, an HPF is applied to the direct-axis current and used to modify the voltage frequency. These various strategies provide valuable insights into the effectiveness of different control methods and can guide the development of more effective and efficient motor control systems.

All of these methods share a common foundation in that they are built upon the concept of compensation control. This type of control is fundamentally based on the parameters of the induction motor, such as its electrical and mechanical characteristics. By adjusting the control inputs based on these parameters, compensation control can effectively manage the operation of the motor and mitigate any undesirable behaviors. However, these methods also involve the use of BPFs and HPFs. These filters are used to process the motor's current and voltage signals, filtering out unwanted noise and fluctuations. While these filters can significantly improve the performance of the control system, they also add a level of complexity to the control algorithms.

This complexity can lead to an increase in computational time, particularly when complex mathematical formulas are involved. This increase in computational time presents a significant challenge when attempting to implement these control methods with low-cost MCUs. These MCUs typically have low clock speeds and limited storage spaces, making them ill-suited for complex computations. As a result, the implementation of these control methods on low-cost MCUs can be a challenging task.

In light of these challenges, this paper proposes a simplified V/f control that can be readily applied in low-cost MCUs. The primary objective of this control strategy is to mitigate the current fluctuations that occur at low operating frequencies. These fluctuations are commonly observed within the variable speed range of induction motors and can lead to unstable motor operation and reduced performance. By effectively mitigating these current fluctuations, the proposed V/f control presents a cost-effective solution for enhancing the performance and reliability of induction motors. This is particularly beneficial in low-frequency operations, where current fluctuations can be particularly problematic.

The simplicity of the proposed control strategy also means that it can be easily implemented on low-cost MCUs, making it a practical solution for a wide range of applications. In conclusion, while traditional control methods based on compensation control and the use of BPFs and HPFs can be effective, they also present challenges in terms of computational complexity and implementation on low-cost MCUs. The proposed V/f control addresses these challenges by offering a simplified and cost-effective solution that enhances the performance and reliability of induction motors, particularly in low-frequency operations.

2. Control Strategy

2.1. Dynamic Equations of the Stator Current of an Induction Motor

The stator current dynamic characteristic equation of an induction motor can be expressed in the form $\dot{x} = Ax + Bu$ as follows [8]:

$$\sigma L_s \frac{di_{ds}}{dt} = -R_s i_{ds} + \omega_e \sigma L_s i_{qs} + v_{ds} \quad (1)$$

$$\sigma L_s \frac{di_{qs}}{dt} = -R_s i_{qs} - \omega_e \sigma L_s i_{ds} - \omega_e \frac{L_m}{L_r} \lambda_{dr} + v_{qs} \quad (2)$$

where σ is $1 - (L_m^2/L_s L_r)$, L_s , L_r , and L_m are stator, rotor, and mutual inductances, R_s is stator resistance, ω_e is electrical angular velocity of the stator, i_{ds} and i_{qs} are the d-axis and q-axis stator currents, λ_{dr} and λ_{qr} are the d-axis and q-axis rotor fluxes, and v_{ds} and v_{qs} are the d-axis and q-axis stator voltages in the synchronous reference frame. For FOC and DTC, the λ_{qr} is 0 and the λ_{dr} is the same as the λ_r , and they are maintained constant. In general V/f control, it is not possible to control the transient-state operation of the induction motor because the input voltage and operating frequency of the induction motor are controlled proportionally. Therefore, the dynamic equation in the steady state ($d/dt = 0$) of V/f control can be expressed as follows:

$$v_{ds} = R_s i_{ds} - \omega_e \sigma L_s i_{qs} \quad (3)$$

$$v_{qs} = R_s i_{qs} + \omega_e L_s i_{ds} \quad (4)$$

The command values of v_{ds}^* and v_{qs}^* for general V/f control using Equations (3) and (4) can be expressed as follows:

$$v_{ds}^* = R_s i_{ds}^* = \text{constant} \quad (5)$$

$$v_{qs}^* = \omega_e^* \sigma L_s i_{ds}^* \approx V_{qs,max} \frac{\omega_e^*}{\omega_b} \quad (6)$$

where the superscript * indicates the command value, $V_{qs,max} = \omega_b^* L_s i_{ds}^*$ is the maximum value of v_{qs} , ω_b is the base frequency, and ω_e^* is the frequency command value of the stator. In [8], a current compensator was added based on the above equation and proposed as follows:

$$v_{ds}^* = R_s i_{ds}^* = \text{constant} \quad (7)$$

$$v_{qs}^* = V_{qs,max} \frac{\omega_e^*}{\omega_b} - \frac{k_1 - k_2 s}{1 + \tau} |i_{ds}| \quad (8)$$

where k_1 and k_2 are the gains of the dynamic compensator and τ is a time constant of a low-pass filter circuit. This control method is effective in suppressing current fluctuations, but the formula is complex and the problem is that the selection of gain values depends on the parameters of the induction motor.

The simplified V/f control based on dynamic current proposed in this paper can be expressed as follows:

$$v_{ds}^* = k_p e(t) + \frac{k_i}{s} e(t) \quad (9)$$

$$v_{qs}^* = \sqrt{v_s^{*2} - v_{ds}^{*2}} \quad (10)$$

where k_p and k_i are the proportional and integral gains of the PI controller for i_{ds} . v_s^* is the command value of the stator input voltage, $e(t)$ is the difference between the command value of i_{ds}^* and the feedback value of i_{ds} , and s is the Laplace operator. Compared to conventional V/f control, the proposed method allows for reduced computation time on the MCUs by utilizing simplified equations.

2.2. Proposed Control for Current Fluctuation Suppression

Figure 1 shows the control block diagram for current fluctuation suppression in an induction motor based on the proposed Equations (9) and (10). Controlling i_{ds} to remain constant ensures that the air gap flux is maintained at a steady level, allowing for the suppression of current fluctuations during transient states.

When the command frequency f_s^* is applied to the V/f curve block, a forced rotation angle θ^* and command input voltage are outputted. By measuring the phase currents of the two-phase stator of the inverter and performing dq transformation based on the forced rotation angle, i_{ds} is calculated. Together with $i_{ds}^* = 0$, it is controlled via a PI controller. The output value of the d-axis PI controller becomes v_{ds}^* . v_{qs}^* is calculated by taking the square root of the difference between the squared v_s^* and the squared v_{ds}^* . v_{ds}^* and v_{qs}^* are

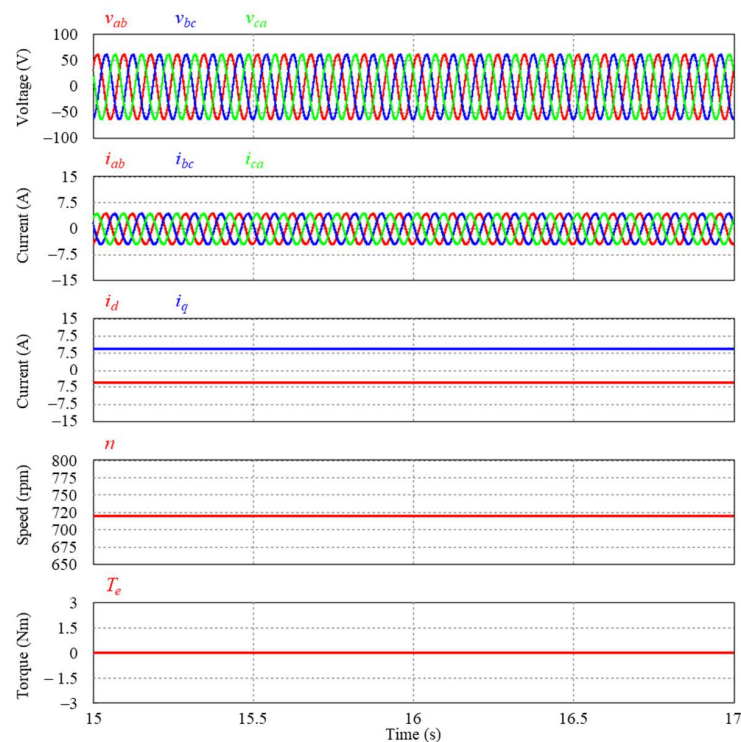
Table 1. Parameters of two induction motors with different rotor moments of inertia.

Item	Unit	Model A	Model B
Rated power	W	746	746
Input voltage	V	220	220
Base frequency	Hz	60	60
Rated speed	rpm	3565	3565
Rated current	A	3.7	3.7
Stator resistance	Ω	1.2	1.2
Stator inductance	mH	107	107
Rotor resistance	Ω	0.57	0.57
Rotor inductance	mH	107	107
Mutual inductance	mH	105.5	105.5
Poles	-	2	2
Moment of inertia of the rotor	kg/m ²	0.0022	0.022

3. Proposed Control Verification

3.1. Characteristic Analysis Based on the Rotor Moment of Inertia

The induction motor was modeled and the effectiveness of the proposed control was validated using PSIM 10, a simulation package that excels in interpreting power electronics and motor control circuits. Figure 2 represents the three line-to-line voltages v_{ab} , v_{bc} , and v_{ca} , three-phase currents i_a , i_b , and i_c , d-axis and q-axis currents i_d and i_q , speed n , and electromagnetic torque T_e when a 44 V, 12 Hz three-phase sinusoidal line-to-line voltage is applied to models A and B, which have different rotor moments of inertia. In the case of Model A, the average root-mean-square (RMS) value of the three-phase current is 3.11 A, and it can be confirmed that there is no variation in each phase current. Since there is no fluctuation in the three-phase current, i_d is -4.35 A and i_q is 6.45 A, remaining stable along with the DC components. The magnitude of the d-axis current and q-axis current is determined by the position of the rotor, which is tracked based on slip. These currents serve a vital role in the operation of the motor and their values can significantly affect the electromagnetic torque performance of the motor.



(a)

Figure 2. Cont.

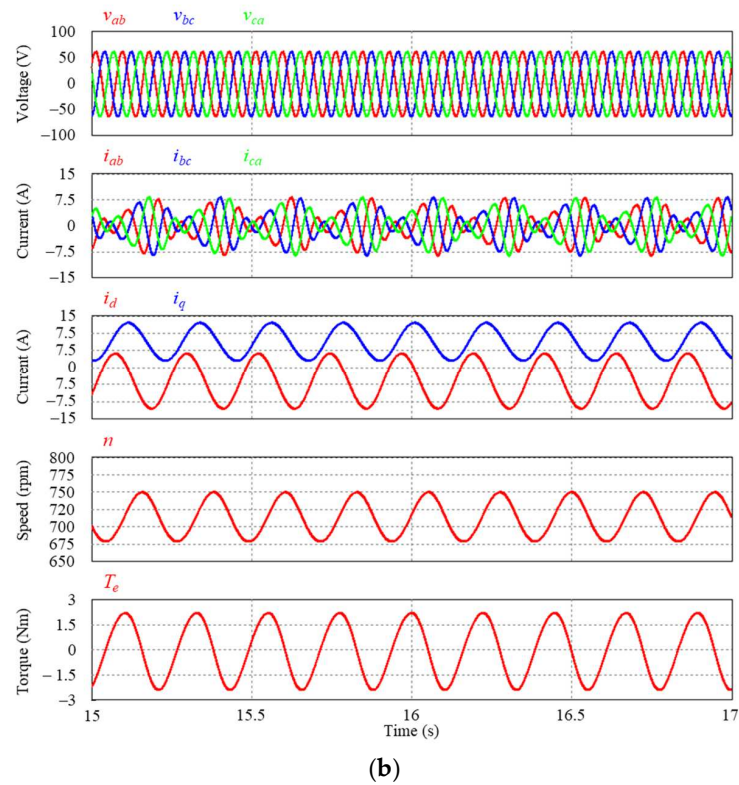


Figure 2. Comparison of output characteristics according to the rotor moment of inertia: (a) Model A; (b) Model B.

When compared to Model A, it can be observed that in Model B, the maximum value of the three-phase current increases up to 8.35 A, indicating approximately 2.25 times greater current fluctuations. The peak-to-peak values of the d-axis and q-axis currents are 5.47 A and 8.05 A, respectively, indicating significant pulsations. Consequently, the peak-to-peak values of the speed and electromagnetic torque are 7.1 rpm and 4.62 Nm, respectively, confirming the occurrence of ripple. As a result, the d-axis and q-axis currents become unstable, ultimately leading to pulsations in the speed and electromagnetic torque. These phenomena eventually manifest as vibrations, thereby inducing instability in the motor drive system.

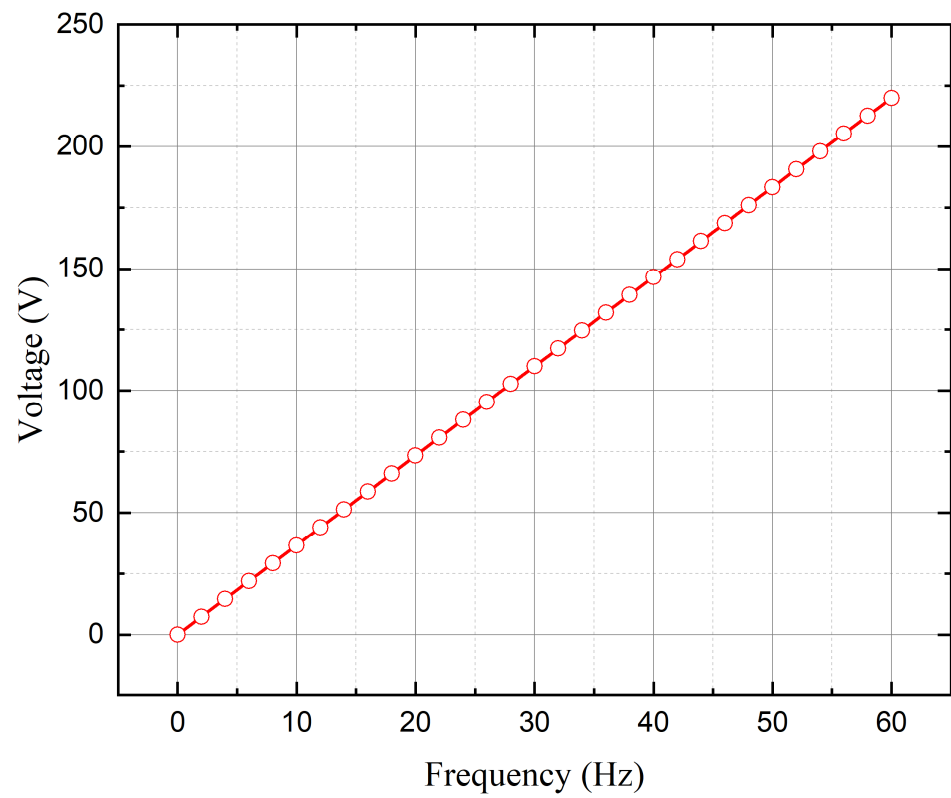
As shown in Figure 3a, when a line-to-line voltage proportional to the frequency is applied, the peak-to-peak value of the phase current, as depicted in Figure 3b, increases from 8 Hz to 16 Hz, with the highest point observed at 12 Hz. To examine the fluctuation rate for each frequency, the formulas for the current fluctuation rate $i_{fluctuation}$ in Figure 3c and speed fluctuation $n_{fluctuation}$ rate in Figure 3d can be expressed as follows:

$$i_{fluctuation} = \frac{|i_{abnormal} - i_{normal}|}{i_{normal}} \times 100 \quad (13)$$

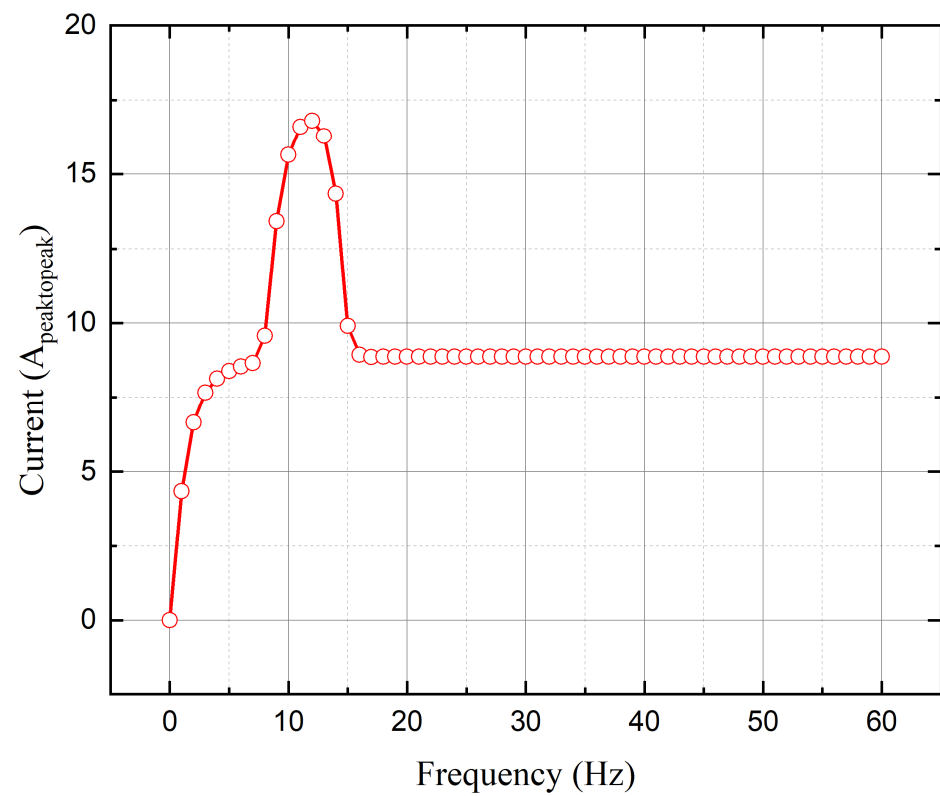
$$n_{fluctuation} = \frac{|n_{max} - n_{min}|}{n_{avg}} \times 100 \quad (14)$$

where $i_{abnormal}$ is the abnormal current, i_{normal} is the normal current or no-load current, n_{max} and n_{min} are the maximum and minimum speeds of the motor, respectively, and n_{avg} is for the average speed of the motor.

The frequency range in which current fluctuation occurs is from 8 Hz to 16 Hz, and the point with the highest current fluctuation rate is at 12 Hz, where the peak-to-peak value of the phase current is 16.8 A, accounting for 90.72%. In terms of the speed fluctuation rate, the highest point is 11.31% at 10 Hz.

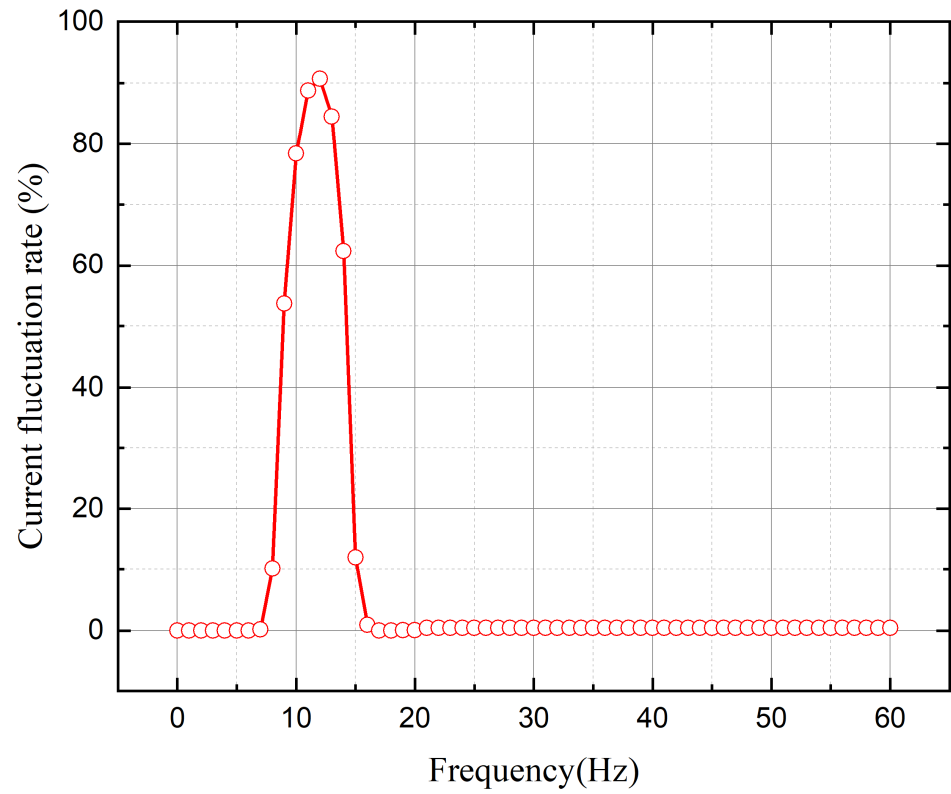


(a)

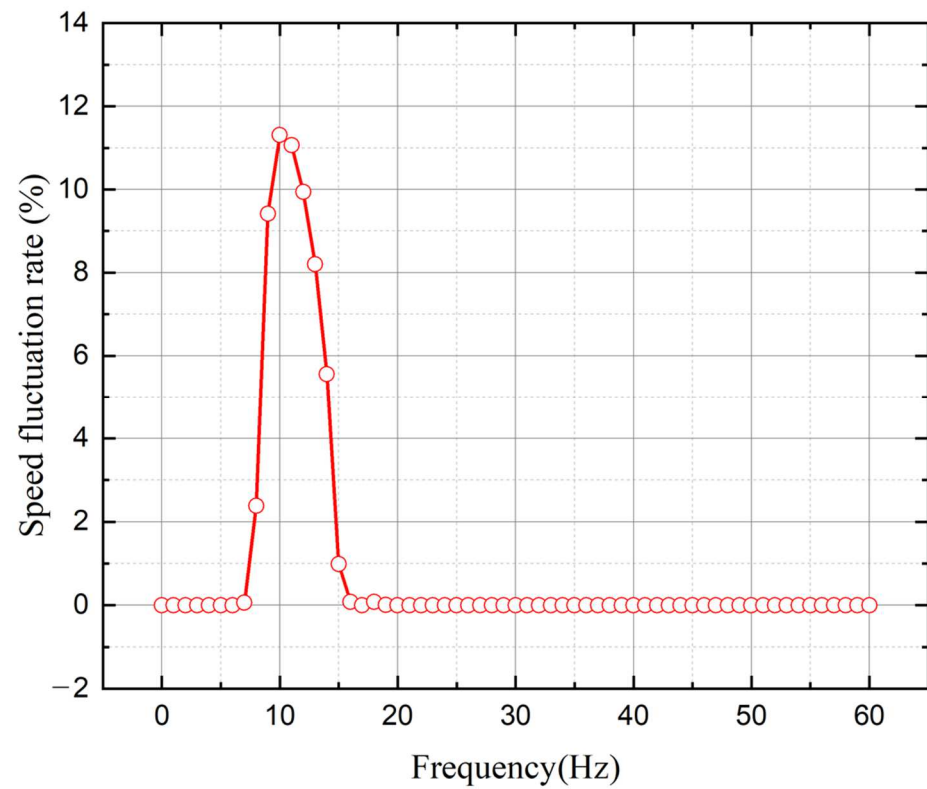


(b)

Figure 3. Cont.



(c)



(d)

Figure 3. Output characteristics of the modeled induction motor according to frequency: (a) line-to-line voltage; (b) peak-to-peak value of phase current; (c) current fluctuation rate; (d) speed fluctuation rate.

3.2. Simulation Results Using PWM Inverter

The control block diagram proposed in Figure 1 was implemented in the PSIM simulation circuit as shown in Figure 4a. The induction motor model with parameters of Model B was connected to the output terminals of a three-phase inverter. The switching frequency of the six IGBTs inside the inverter was set to 8 kHz, and the control interrupt period was set to 0.125 ms, which is the inverse of the switching frequency. All blocks in the simulation circuit operate synchronously with the interrupt period. When the command frequency is input to the frequency ramp, a reference frequency with a slope of 6 Hz per second is outputted. According to the traditional V/f curve, where the command frequency R_Freq is input to the V/f generator, the output phase voltage V_s and frequency F_{out} are produced. These values are inputted into the Forced Rotating Angle Generator to produce the forced electrical rotation angle FRA. The FRA is utilized as the angle for abc-to-dq transformation and dq-to-abc transformation. In the proposed control block, the PI controller is configured to maintain a constant d-axis feedback current i_{d_P} , calculated from the abc-to-dq transformation using the measured two-phase currents. The output of the PI controller is the d-axis voltage v_d . The q-axis voltage is calculated as the square root of the difference between the square of v_s and the square of v_d . The outputted v_d and v_q are transformed back to phase voltages v_a , v_b , and v_c through abc-to-dq transformation and then inputted to the SVPWM block. The three outputs of the SVPWM block are transformed into six PWM waveforms through comparators and fed into the gate inputs of the six IGBTs inside the inverter.

Figure 4b,c presents a comparison of the output characteristics of Model B at the frequencies of 11 Hz and 12 Hz applied to a PWM inverter. When the proposed control is not applied, unstable fluctuations occur in phase current $i_{a_without}$, d-axis current $i_{ds_without}$, electromagnetic torque $T_{e_without}$, and speed $n_{without}$. Compared to the results without the proposed control, the proposed control shows stable output characteristics in phase current i_{a_with} , d-axis current i_{ds_with} , electromagnetic torque T_{e_with} , and speed n_{with} .

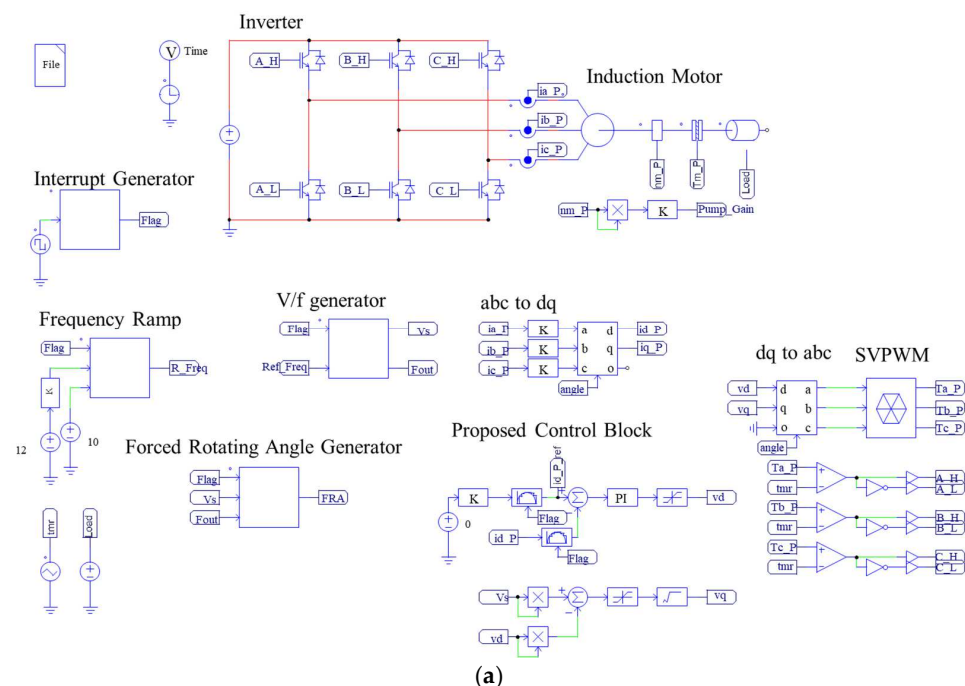
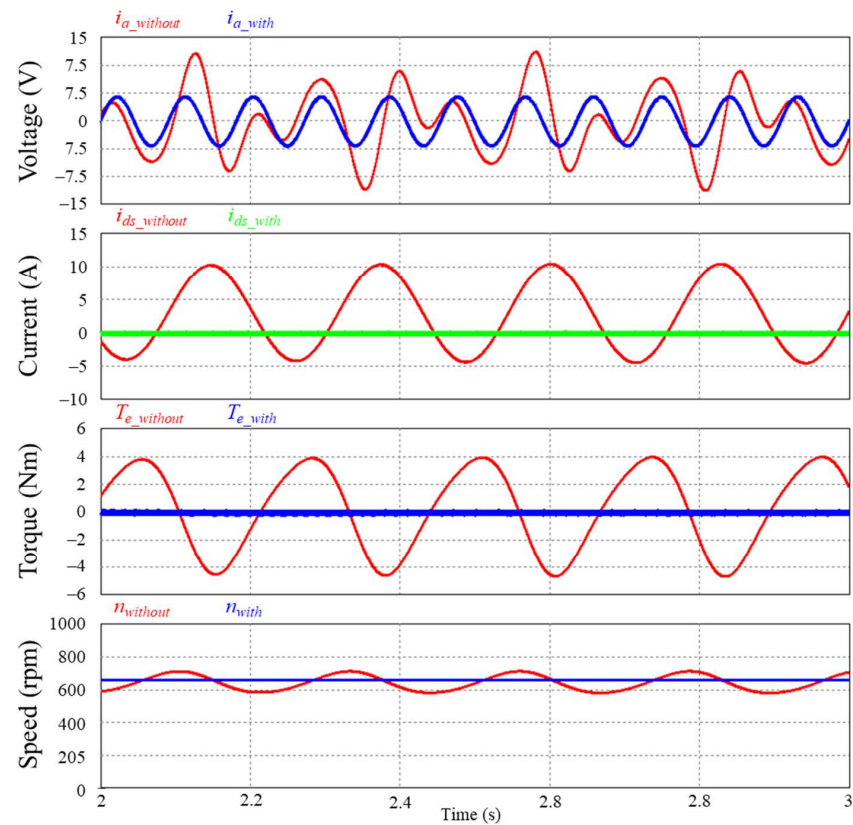
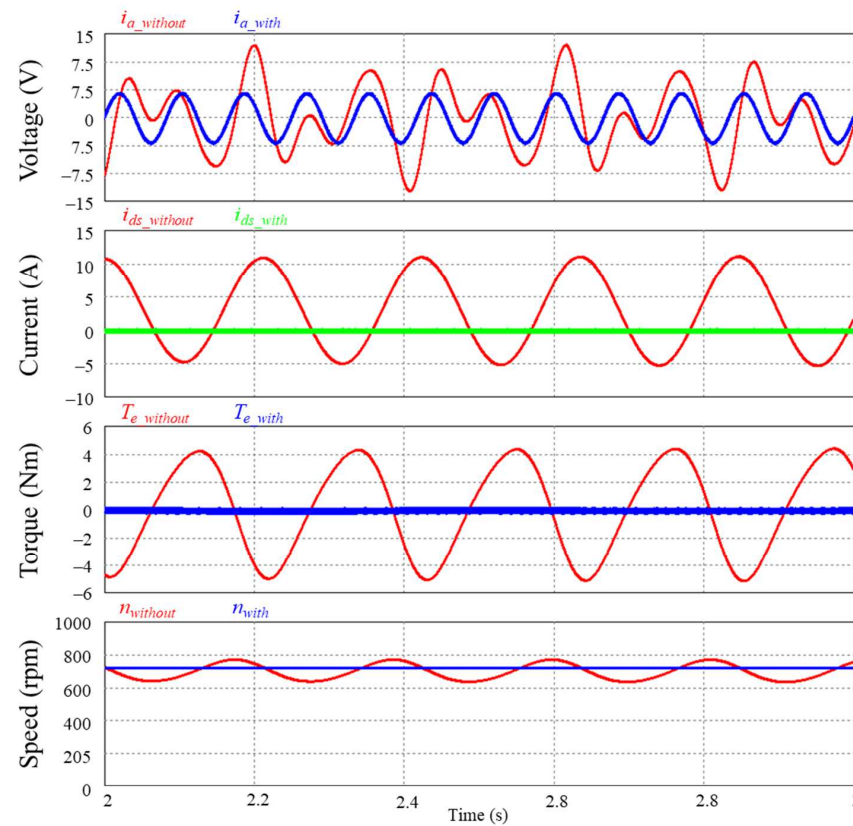


Figure 4. Cont.



(b)



(c)

Figure 4. Simulation results of proposed control: (a) simulation circuit of Model B and inverter considering load; (b) output characteristics of the induction motor without and with proposed control at 11 Hz; (c) output characteristics of the induction motor without and with proposed control at 12 Hz.

Figure 5 represents a comparative analysis of simulations without and with the proposed control applied to a PWM inverter, depending on the frequency. In Figure 5a, without the proposed control, the current fluctuation rate is over 10% in the 8~20 Hz range, and the maximum current fluctuation rate is 166.48% at 15 Hz. When the proposed control is applied, it can be confirmed that the current fluctuation rate is attenuated to 1.5~3.6% in all frequency ranges. Figure 5b is a curve comparing the speed fluctuation rate. The existing control increased up to a maximum of 20.7% at 10 Hz, but in the case of the proposed control, it was confirmed to be within 0.35% in all frequency ranges.

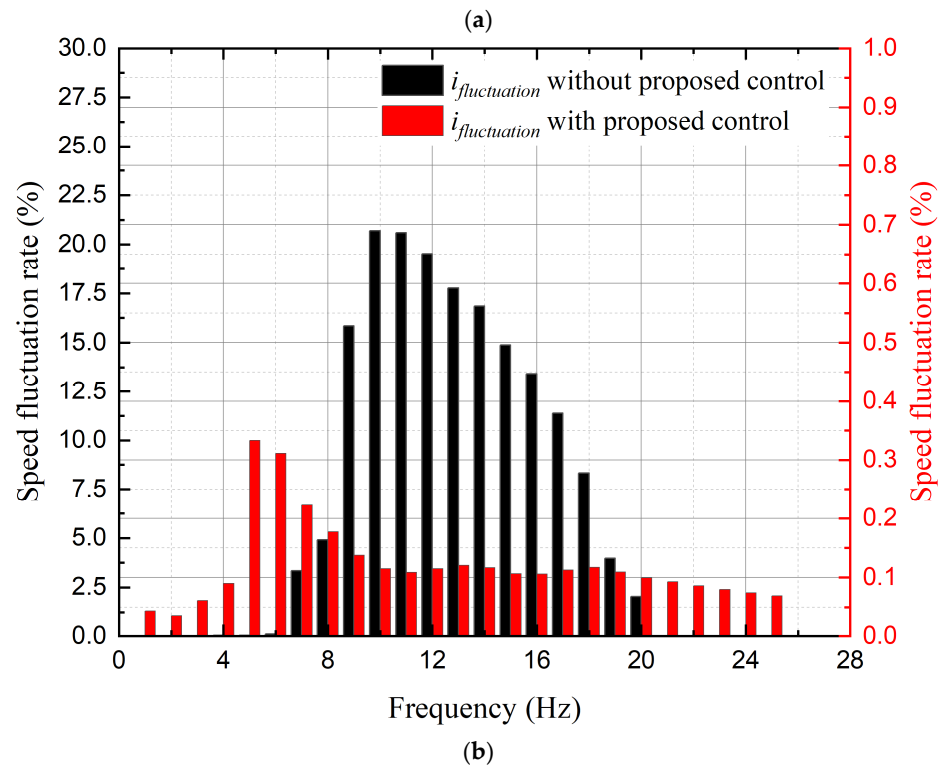
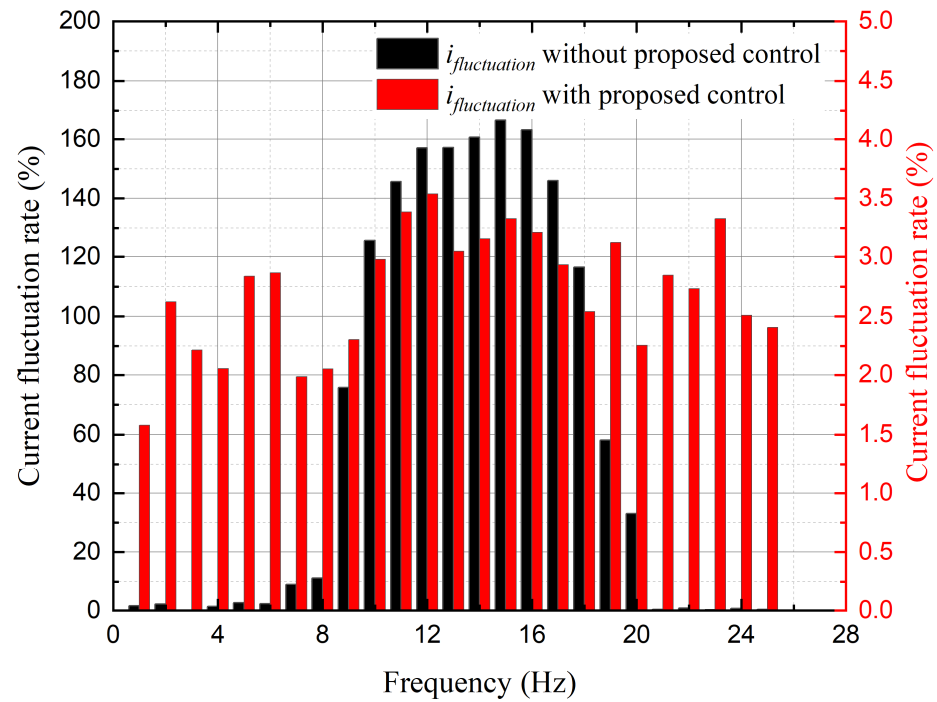


Figure 5. Cont.

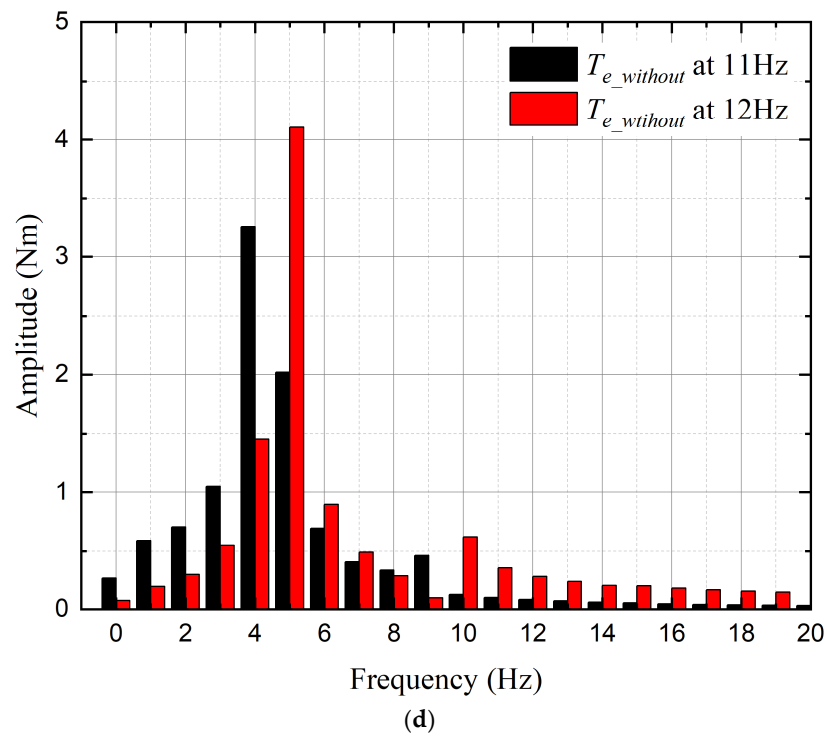
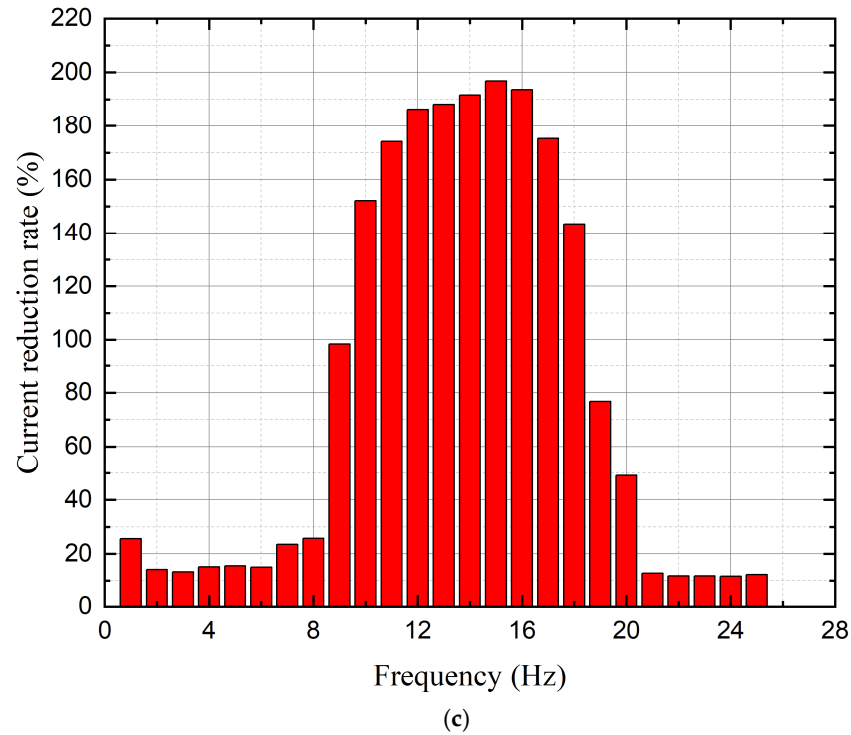


Figure 5. Comparative analysis of the results depending on the presence or absence of the proposed control in the frequency range where current fluctuations occur: (a) current fluctuation rate; (b) speed fluctuation rate; (c) current reduction rate; (d) harmonic analysis of electromagnetic torque.

Figure 5c is a curve comparing the current reduction rate without and with the proposed control. The formula for the current reduction rate is as follows:

$$i_{reduction} = \frac{|i_{without} - i_{with}|}{i_{with}} \times 100 \tag{15}$$

where $i_{without}$ is the peak-to-peak value of the phase current when the proposed control is not applied, and i_{with} represents the peak-to-peak value of the phase current when the proposed control is applied. The current fluctuation reduction is achieved in the range of 8 Hz to 20 Hz,

and the frequency with the largest reduction rate is 15 Hz, which is 196.84%. In other frequency ranges, it means that there is no current fluctuation. Figure 5d shows the results of the harmonic analysis of electromagnetic torque at 11 Hz and 12 Hz. For 11 Hz, the highest electromagnetic torque magnitude is 3.25992 Nm at 3 Hz, and for 12 Hz, it is 4.10676 Nm at 4 Hz. When the proposed control is applied, it can be confirmed that the operation is stable as no magnitude occurs in all frequency ranges of the harmonic analysis results of 11 Hz and 12 Hz. These values ultimately cause vibration and noise in the induction motor, leading to system instability.

3.3. Experimental Results

Figure 6 illustrates the experimental setup for measuring the current fluctuation rate to validate the effectiveness of the proposed control. The phase current was measured using an oscilloscope according to the frequency in a no-load condition of a 746 W induction motor.

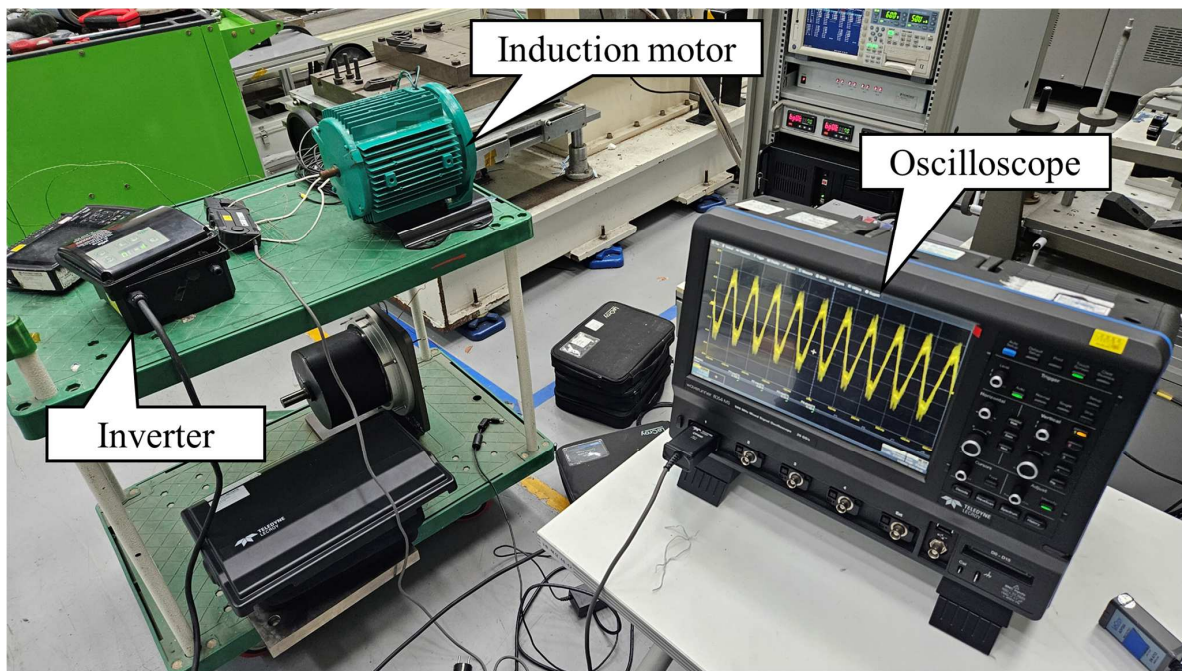


Figure 6. Experimental setup for measuring current fluctuation rate.

The frequency range in which current fluctuations occur was confirmed as shown in Figure 7, increasing by 1 Hz from 10 Hz to 19 Hz. The area where current fluctuations occur is from 10 Hz to 19 Hz, and this frequency range can vary depending on the parameter changes due to the temperature of the motor and the change in inertial load due to the transient state of speed. Figure 8 demonstrates the stability of the phase current across frequencies when the proposed control is applied.

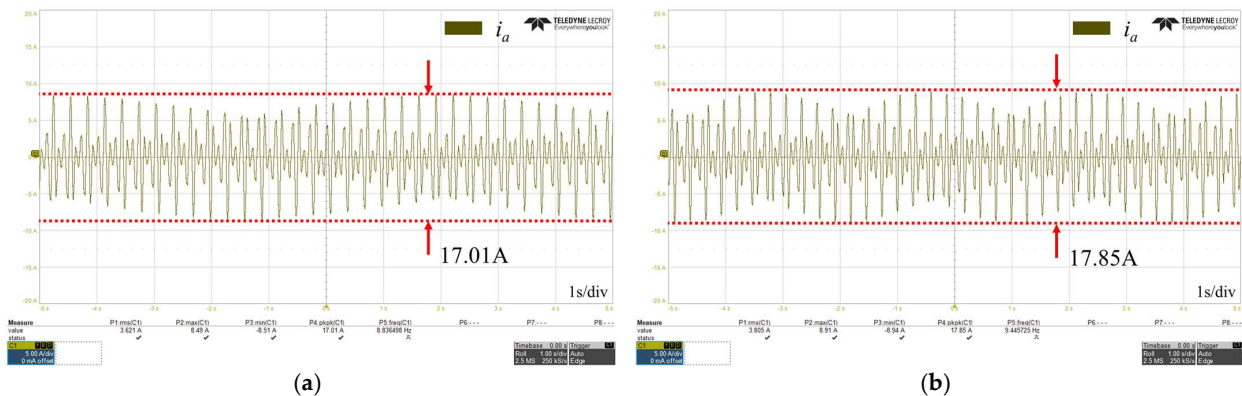


Figure 7. Cont.

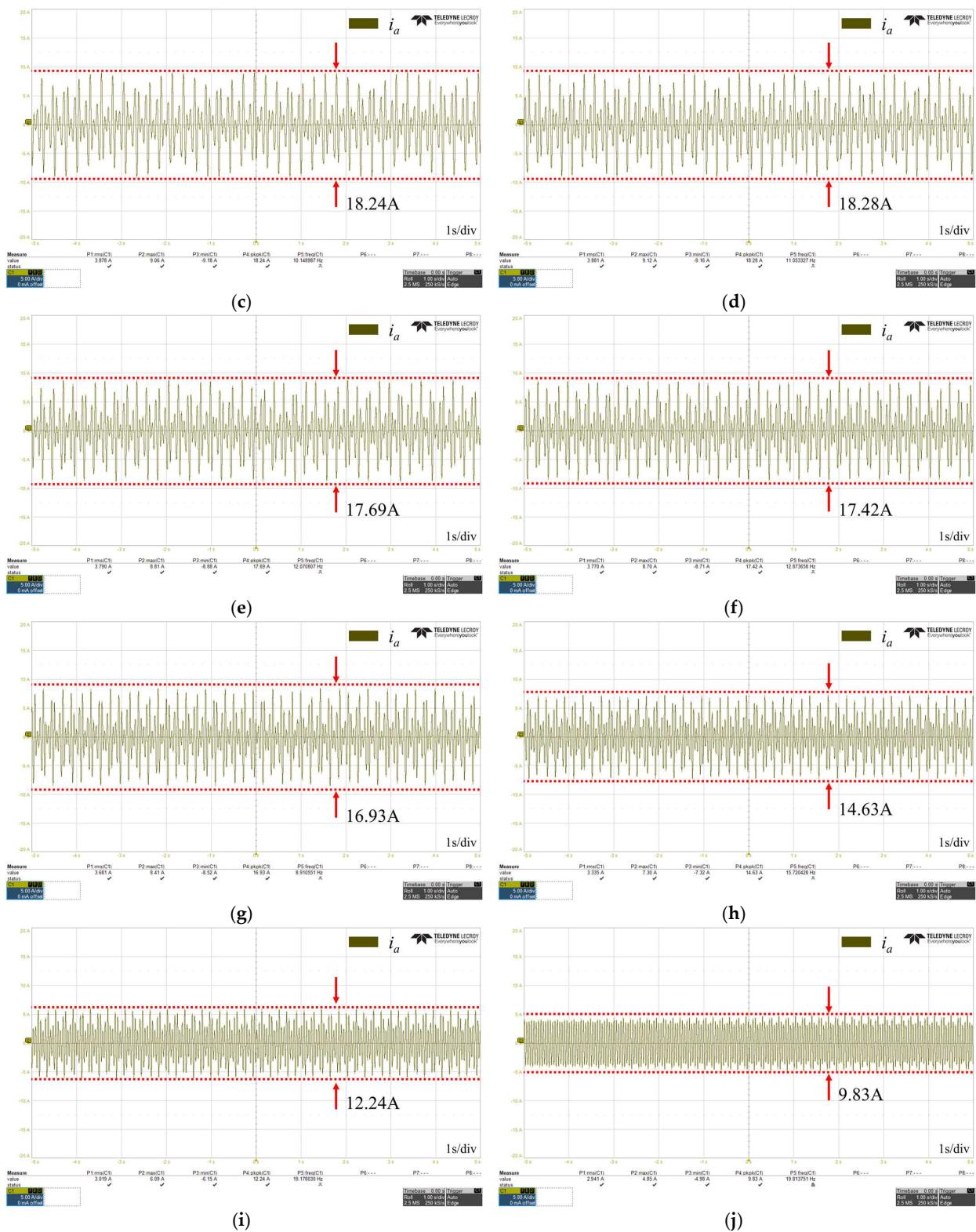


Figure 7. Experimental results of phase current fluctuation without the proposed control: (a) 10 Hz; (b) 11 Hz; (c) 12 Hz; (d) 13 Hz; (e) 14 Hz; (f) 15 Hz; (g) 16 Hz; (h) 17 Hz; (i) 18 Hz; (j) 19 Hz.

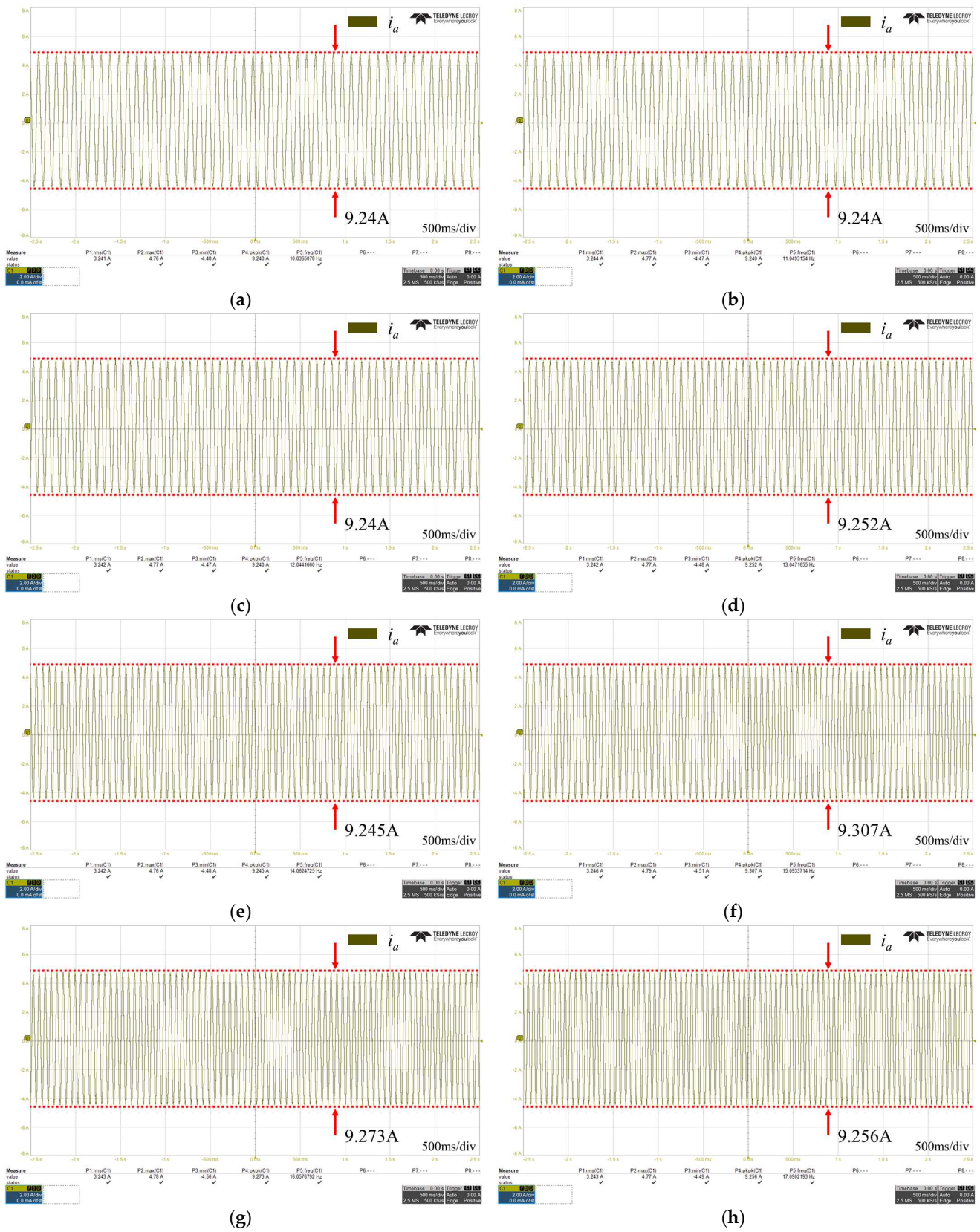


Figure 8. Cont.

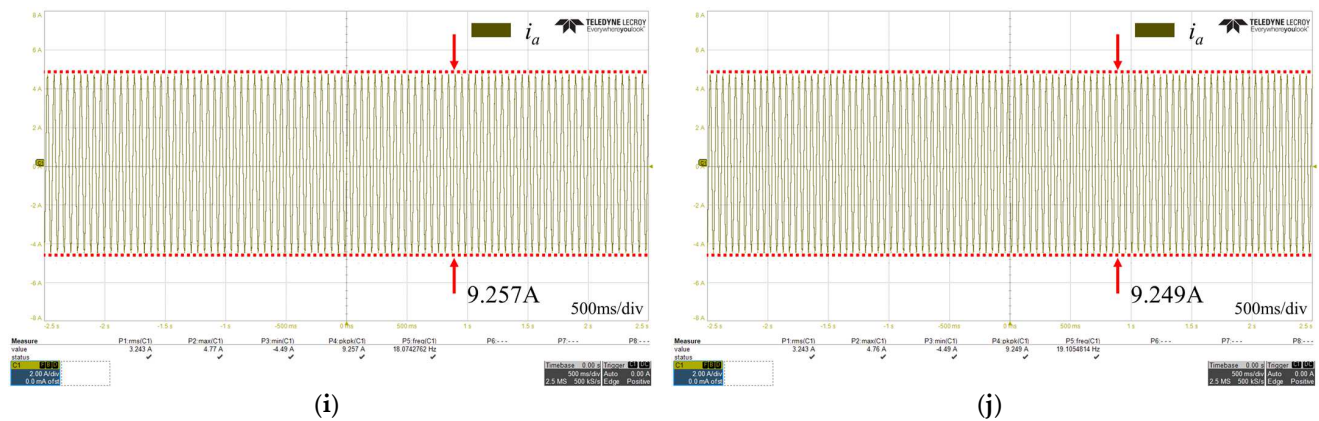


Figure 8. Experimental results of phase current fluctuation with the proposed control: (a) 10 Hz; (b) 11 Hz; (c) 12 Hz; (d) 13 Hz; (e) 14 Hz; (f) 15 Hz; (g) 16 Hz; (h) 17 Hz; (i) 18 Hz; (j) 19 Hz.

Table 2 represents the fluctuation rate of the phase current when the phase current is selected as the normal current according to the frequency when FOC control is applied. In FOC control, the d-axis current is set based on the parameters of the induction motor. In this experiment, the peak-to-peak value of no-load current was derived as 8.57A using the auto-tuning function of the Yaskawa A1000 drive (Yaskawa, Fukuoka, Japan). Using Equation (13), it was confirmed that the current fluctuation was suppressed to within approximately $8\% \pm 0.6\%$. The presence of a current fluctuation rate is due to the difference caused by the limitations of ADC and operation control resolution due to the use of a low-cost MCU. However, this difference is not significant, and the results sufficiently validate the effectiveness of the proposed control.

Table 2. Experimental results of current fluctuation rate depending on frequency without and with proposed control.

Frequency (Hz)	Normal Current ($A_{\text{peaktopeak}}$)	Without Proposed Control		With Proposed Control	
		Fluctuation Current ($A_{\text{peaktopeak}}$)	Current Fluctuation Rate (%)	Fluctuation Current ($A_{\text{peaktopeak}}$)	Current Fluctuation Rate (%)
10	8.573	17.01	98.41	9.24	7.78
11	8.573	17.85	108.21	9.24	7.78
12	8.573	18.24	112.76	9.24	7.78
13	8.5701	18.28	113.3	9.252	7.96
14	8.5701	17.69	106.41	9.245	7.88
15	8.573	17.42	103.2	9.307	8.56
16	8.573	16.93	97.48	9.273	8.17
17	8.573	14.63	70.65	9.256	7.97
18	8.573	12.24	42.77	9.257	7.98
19	8.5701	9.83	14.70	9.249	7.92

4. Conclusions

This paper presents a novel, simplified, and highly effective control strategy specifically designed for suppressing current fluctuations in the low-frequency range of open-loop V/f control in induction motor drives. The strategy is devised and involves applying the command frequency to the V/f curve block. This block, in turn, outputs two crucial parameters: the forced rotation angle and the command input voltage.

The inverter, a key component in the system, measures the phase current of the two-phase stator. It then performs the dq transformation, a mathematical operation that is based on the stator's forced rotation angle. This transformation is used to calculate the d-axis current, a critical parameter in the control of the motor. This calculated d-axis current is then regulated to zero using a PI controller. The output of this controller

becomes the d-axis command voltage. The output of this controller is designated as the d-axis command voltage, and the q-axis command voltage is determined by the difference between this command voltage and the command input voltage. This q-axis command voltage is then input to SVPWM through the $\alpha\beta$ transformation. One of the significant advantages of this proposed method is that it does not require complex formulas to track the slip of the induction motor. This simplifies the control strategy and makes it more robust and easier to implement. The method has been proven to effectively suppress current fluctuations, enhancing the stability and performance of the motor. Experimental results provide strong evidence of the effectiveness of the proposed method. The results show that the proposed method reduces current fluctuation rates to below 8.6% across all frequencies in the 10~19 Hz range. This is a substantial improvement from the over 10% and up to 113.3% fluctuation rates observed without the proposed control. The simplicity of the proposed method, which does not require precise motor parameters or complex filter design and implementation, makes it a practical solution for enhancing the stability of induction motor drive systems. Furthermore, the proposed control, composed of simpler equations and devoid of digital filters, can reduce the computation time of the MCU, enabling the use of low-cost MCUs. This is a significant advantage in cost-sensitive applications. Future research will focus on suppressing current fluctuation rates under load conditions across all frequency ranges and further reducing current fluctuation rates. This will further enhance the performance and reliability of induction motor drive systems, contributing to the development of more efficient and sustainable industrial systems.

Author Contributions: Conceptualization, S.-A.K.; methodology, S.-A.K.; software, D.-H.S.; validation, S.-A.K.; formal analysis, D.-H.S.; investigation, D.-H.S.; writing—original draft preparation, D.-H.S.; writing—review and editing, S.-A.K.; visualization, S.-A.K. All authors have read and agreed to the published version of the manuscript.

Funding: This work was partly supported by the Collabo R&D Program of MSS (RS-2023-00221749) and the Full Cycle Technology Development of MOTIE (RS-2023-00255506).

Data Availability Statement: Data are contained within the article.

Conflicts of Interest: Dong-Hyeok Son is employed at Sansystech. The authors declare no conflict of interest.

References

1. Teixeira, A.C.R.; Sodré, J.R. Impacts of Replacement of Engine Powered Vehicles by Electric Vehicles on Energy Consumption and CO₂ Emissions. *Transp. Res. Part D Transp. Environ.* **2018**, *59*, 375–384. [\[CrossRef\]](#)
2. Gobbi, M.; Sattar, A.; Palazzetti, R.; Mastinu, G. Traction Motors for Electric Vehicles: Maximization of Mechanical Efficiency—A Review. *Appl. Energy* **2024**, *357*, 122496. [\[CrossRef\]](#)
3. Konda, Y.R.; Ponnaganti, V.K.; Reddy, P.V.S.; Singh, R.R.; Mercorelli, P.; Gundabattini, E.; Solomon, D.G. Thermal Analysis and Cooling Strategies of High-Efficiency Three-Phase Squirrel-Cage Induction Motors—A Review. *Computation* **2024**, *12*, 6. [\[CrossRef\]](#)
4. Lee, K.; Han, Y. Reactive-Power-Based Robust MTPA Control for V/f Scalar-Controlled Induction Motor Drives. *IEEE Trans. Ind. Electron.* **2022**, *69*, 169–178. [\[CrossRef\]](#)
5. Lipo, T.A.; Krause, P.C. Stability analysis of a rectifier-inverter induction motor drive. *IEEE Trans. Power Appar. Syst.* **1969**, *PAS-88*, 55–66. [\[CrossRef\]](#)
6. Ueda, R.; Sonoda, T.; Takata, S. Experimental Results and Their Simplified Analysis on Instability Problems in PWM Inverter Induction Motor Drives. *IEEE Trans. Ind. Appl.* **1989**, *25*, 86–95. [\[CrossRef\]](#)
7. Oteafy, A.; Chiasson, J. A study of the Lyapunov stability of an open-loop induction machine. *IEEE Trans. Control Syst. Technol.* **2010**, *18*, 1469–1476. [\[CrossRef\]](#)
8. Jung, J.-H.; Jeong, G.-Y.; Kwon, B.-H. Stability Improvement of V/f Controlled Induction Motor Drive Systems by a Dynamic Current Compensator. *IEEE Trans. Ind. Electron.* **2004**, *51*, 930–933. [\[CrossRef\]](#)
9. Samal, K.B.; Pati, S.; Sharma, R. Integration of a Proton Exchange Membrane Fuel Cell System for Voltage and Frequency Stabilization in a Micro Hydro System. *E-Prime-Adv. Electr. Eng. Electron. Energy* **2024**, *7*, 100428. [\[CrossRef\]](#)
10. Zagirnyak, M.; Korenkova, T.; Kovalchuk, V.; Szczęsny, A.; Korzeniewska, E. The Analysis of Operation Modes of Variable Speed Pump Units with Different Circuits of Turbomachine Connection. *Energies* **2024**, *17*, 882. [\[CrossRef\]](#)

11. Shakweh, Y. Variable Speed Drive Types and Specifications. In *Power Electronics Handbook*; Butterworth-Heinemann: Oxford, UK, 2024; pp. 1037–1072.
12. Chuensiri, S.; Katchasuwannanee, K.; Wisessint, A.; Jotisankasa, A.; Soralump, C.; Siriyakorn, V.; Sanposh, P. Implementation of Adaptive Network-Based Fuzzy Inference for Hybrid Ground Source Heat Pump. *IEEE Access* **2024**, *12*, 21052–21069. [[CrossRef](#)]
13. Gao, M.; Wang, Q.; Shan, X.; Li, Q.; Zhang, L. Application of Hydraulic Energy-Saving Technology in the Teaching, Research, and Practice of Mechanical Engineering. *Sustainability* **2024**, *16*, 1315. [[CrossRef](#)]
14. Wang, S.; Prystupa, D.; Bao, Y.; Varvolik, V.; Buticchi, G.; Zhang, H.; Degano, M. Comprehensive Modulation Strategies for Synchronous Reluctance Motor Drives Used in Weak Grids. *Energies* **2024**, *17*, 615. [[CrossRef](#)]
15. Elgbaily, M.; Anayi, F.; Alshbib, M.M. A Combined Control Scheme of Direct Torque Control and Field-Oriented Control Algorithms for Three-Phase Induction Motor: Experimental Validation. *Mathematics* **2022**, *10*, 3842. [[CrossRef](#)]
16. El Ouanjli, N.; Derouich, A.; El Ghzizal, A. Modern Improvement Techniques of Direct Torque Control for Induction Motor Drives—A Review. *Prot. Control Mod. Power Syst.* **2019**, *4*, 11. [[CrossRef](#)]
17. Narayana, K.S.; Surekha, P.; Prasuna, P.V. A New FOC Approach of Induction Motor Drive Using DTC Strategy for the Minimization of CMV. *Int. J. Power Electron. Drive Syst.* **2013**, *3*, 241. [[CrossRef](#)]
18. Jnayah, S.; Khedher, A. DTC of Induction Motor Drives Fed by Two and Three-Level Inverter: Modeling and Simulation. In Proceedings of the 2019 19th International Conference on Sciences and Techniques of Automatic Control and Computer Engineering (STA), Sousse, Tunisia, 24–26 March 2019.
19. Casadei, D.; Profumo, F.; Serra, G.; Tani, A. FOC and DTC: Two Viable Schemes for Induction Motors Torque Control. *IEEE Trans. Power Electron.* **2002**, *17*, 779–787. [[CrossRef](#)]
20. Graciola, C.L.; Goedtel, A.; Angélico, B.A. Energy Efficiency Optimization Strategy for Scalar Control of Three-Phase Induction Motors. *J. Control Autom. Electr. Syst.* **2022**, *33*, 1032–1043. [[CrossRef](#)]
21. Hoang, M.H.; Ahn, H.J. RTC (Reaction Torque Compensated) Induction Motor and Its Open-Loop Control. *JMST Adv.* **2019**, *1*, 23–30. [[CrossRef](#)]
22. Duranay, Z.B.; Guldemir, H.; Tuncer, S. Implementation of a V/F Controlled Variable Speed Induction Motor Drive. *EMITTER Int. J. Eng. Technol.* **2020**, *8*, 35–48. [[CrossRef](#)]
23. Selvan, S.; Venkadesan, A.; Sedhuraman, K. V/F Speed Control of Three-Phase and Five-Phase Induction Motor Drive: A Comparative Study. In *Advances in Electrical and Computer Technologies*; Sengodan, T., Murugappan, M., Misra, S., Eds.; ICAECT 2020, Lecture Notes in Electrical Engineering; Springer: Singapore, 2021; Volume 711.
24. Munoz-Garcia, A.; Lipo, T.A.; Novotny, D.W. A New Induction Motor V/f Control Method Capable of High-Performance Regulation at Low Speeds. *IEEE Trans. Ind. Appl.* **1998**, *34*, 813–821. [[CrossRef](#)]
25. Shetty, A.; Suryanarayana, K. Variable Frequency and Voltage Control of Induction Motor for Electric Vehicles. In *Advances in Renewable Energy and Electric Vehicles*; Sanjeevikumar, P., Prabhu, N., Suryanarayana, K., Eds.; Lecture Notes in Electrical Engineering; Springer: Singapore, 2022; Volume 767.
26. Carbone, L.; Cosso, S.; Kumar, K.; Marchesoni, M.; Passalacqua, M.; Vaccaro, L. Stability Analysis of Open-Loop V/Hz Controlled Asynchronous Machines and Two Novel Mitigation Strategies for Oscillations Suppression. *Energies* **2022**, *15*, 1404. [[CrossRef](#)]
27. Guha, A.; Narayanan, G. Small-Signal Stability Analysis of an Open-Loop Induction Motor Drive Including the Effect of Inverter Deadtime. *IEEE Trans. Ind. Appl.* **2016**, *52*, 242–253. [[CrossRef](#)]
28. Hinkkanen, M.; Tiitinen, L.; Mölsä, E.; Harnefors, L. On the Stability of Volts-Per-Hertz Control for Induction Motors. *IEEE J. Emerg. Sel. Top. Power Electron.* **2022**, *10*, 1609–1618. [[CrossRef](#)]
29. Xiang, Y.Q. Instability Compensation of V/Hz PWM Inverter-Fed Induction Motor Drives. In Proceedings of the IEEE Conference Record Industrial Applications Conference 32nd IAS Annual Meeting, New Orleans, LA, USA, 5–9 October 1997; pp. 613–620.
30. Ma, Z.; Lin, F.; Zheng, T.Q. A New Stabilizing Control Method for Suppressing Oscillations of V/Hz Controlled PWM Inverter-Fed Induction Motors Drives. In Proceedings of the IEEE 37th Power Electronics Specialists Conference, Jeju, Republic of Korea, 18–22 June 2006; pp. 1–4.
31. Suzuki, K.; Saito, S.; Kudor, T.; Tanaka, A.; Andoh, Y. Stability improvement of V/F controlled large capacity voltage-source inverter fed induction motor. In Proceedings of the Conference Record of the 2006 IEEE Industry Applications Conference Forty-First IAS Annual Meeting, Tampa, FL, USA, 8–12 October 2006; pp. 90–95.
32. Qian, Z.; Yao, W.; Lee, K. Stability analysis and improvement of V/Hz controlled adjustable speed drives equipped with small DC-link thin film capacitors. In Proceedings of the 2018 IEEE Applied Power Electronics Conference and Exposition (APEC), San Antonio, TX, USA, 4–8 March 2018; pp. 861–866.
33. Zhang, S.; Kang, J.; Yuan, J. Analysis and suppression of oscillation in V/F controlled induction motor drive systems. *IEEE Trans. Transp. Electrification* **2022**, *8*, 1566–1574. [[CrossRef](#)]

Disclaimer/Publisher’s Note: The statements, opinions and data contained in all publications are solely those of the individual author(s) and contributor(s) and not of MDPI and/or the editor(s). MDPI and/or the editor(s) disclaim responsibility for any injury to people or property resulting from any ideas, methods, instructions or products referred to in the content.